# J4J.5 Comparisons of Simulated Kinematic and Moisture Fields with Airborne In-situ and Doppler Radar Observations in a Convective Cold Front over the Eastern Pacific Ocean

P. Ola G. Persson[1], J.-W. Bao[2], S. Braun[3], D. Jorgensen[4], B. Walter[5], and M. Han[3]
[1]CIRES/University of Colorado/NOAA/ETL, Boulder, CO
[2]NOAA/ETL, Boulder, CO
[3]NASA/GSFC, Greenbelt, MD
[4]NOAA/NSSL, Norman, OK
[5]Northwest Research Associates, Bellevue, WA

## 1. INTRODUCTION

During the Pacific Landfalling Jets (PACJET) field program, the National Oceanic and Atmospheric Administration (NOAA) P-3 aircraft sampled a strong, convective cold front over the eastern Pacific Ocean off the coast of Southern California on Feb. 19, 2001. The flight track was such to permit both along-front and cross-front cross-sections of in-situ thermodynamic and kinematic data as well as obtaining Doppler radar data from the intense precipitation. Reflectivities along the narrow cold-frontal rainband (NCFR) reached over 50 dBz, and the NCFR was organized into typical core and gap regions. This storm has been the focus of several studies because of its strong convective nature, and because of the availability of the NOAA P-3 data nearly coincident with overpasses of the Tropical Rainfall Measuring Mission (TRMM) satellite and the QuikScat satellite. Jorgensen et al (2003) described the salient characteristics of the frontal convection, and related the along-front variation of the updraft slope to the prefrontal vertical shear and, hence, to the theory presented by Rotunno et al (1988). Persson et al (2004) noted systematic differences in the low-level stress and the wind directions, and suggested that these differences cause systematic errors in the QuikScat wind directions ahead of and behind frontal systems.

In this and a companion paper (Han et al 2005), a fine-scale MM5 simulation is used to link the observations available from the TRMM satellite and the P-3 aircraft. Han et al (2005) describe the comparison between the TRMM observations and the MM5 simulation; in this paper, we validate the MM5 simulation with the Doppler radar and in-situ observations from the P-3, focusing on the aspects related to the TRMM observations of this case. Of particular interest are the mesoscale kinematic and thermodynamic structures associated with the NCFR and the broader upper-level cloud shield bracketing the cold front.

*Corresponding author address:* Dr. Ola Persson, CIRES/NOAA/ETL, 325 Broadway, Boulder, CO 80305; e-mail: opersson@cires.colorado.edu.

## 2. OBSERVATIONS

### 2.1 DATA SOURCES

PACJET was conducted over the eastern North Paciifc Ocean during January and February of 2001 and 2002. A key platform used during PACJET was the NOAA P-3 research aircraft. Measurements from the P-3 aircraft included basic temperature, humidity, and wind information, gust-probe data (three-dimensional wind components and temperature data at 40 Hz), radar wind and reflectivity data from the X-band Doppler tailradar, and dropsonde data. The Doppler radar data, only obtainable in precipitating areas, was processed as described by Jorgensen *et al.* (2003), producing a three-dimensional volume of u, v, w, and reflectivity data with a 1x1 km horizontal resolution and a vertical resolution of 250 m.

In-situ observations in a cross-section from just east of the cold front to west of the main cloud shield are provided by two P-3 aircraft soundings, two dropsondes, a high-level flight leg at 5.3 km towards the west and a low-level flight leg at 300 m towards the east, all completed within the time period 0553-0808 UTC, Feb. 19. The aircraft track relative to the cloud image is shown in Fig. 1. IR satellite images are only available for 0400, 0800, and 0830 UTC, so the 0800 UTC image is used, and the aircraft/dropsonde position is time-to-space adjusted to this time using a system phase velocity of 18 m $s^{-1}$ from 235°. Note that the western 25% of the P3 track was west of the main upper-level cloud shield (Fig. 1), but both dropsondes were within the cloud shield. The eastern end of the track is just on the warm side of the surface cold front (e.g., see Fig. 4), but is well within the upper-level cloud shield associated with this storm. The cloud-top radiative temperatures near the flight track in Fig. 1 are about -40°C, while the coldest temperatures (the blues) are about -50°C. Both of these temperatures are substantially lower than those measured by the aircraft (see Fig. 2a), indicating that the upper leg of the aircraft was well below cloud top

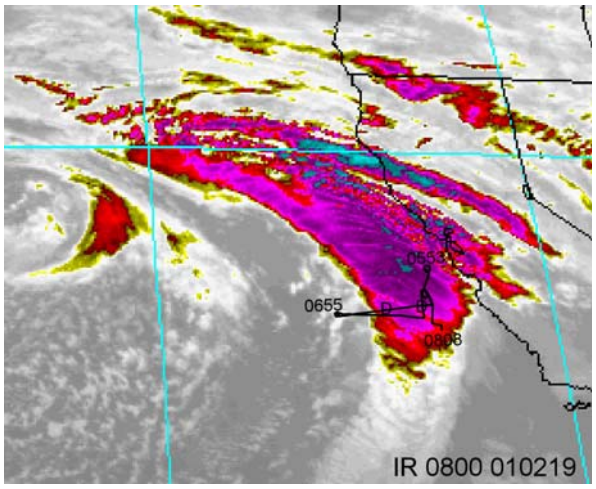


*Fig. 1: P-3 flight track between 0553-0808 UTC Feb. 19 overlaid on IR satellite image at 0800 UTC. The track is time-space adjusted to 0800 UTC using 18 m/s from 235°. The times of the flight- track end points are marked, as are the locations of the dropsondes (D).*

## 2.2 DATA ANALYSES

### 2.2.1 In-situ observations of the frontal and post-frontal regions

The freezing level was at 2 km in the warm sector and at 1.65 km near the western end of the flight track (Fig. 2a). The temperatures along the top leg of the flight track at 5.3 km are -19°C - -24°C. Though the $RH_w$ is only between 80-90% along much of this leg, the air is saturated or supersaturated with respect to ice ($RH_i$ > 100%; Fig. 3). Ice clouds roughly correspond to $RH_w$ > 80% above about 3 km, for which temperatures range from -6°C to -10°C (Fig. 3b). The area of $RH_w$ > 90% near the back edge of the upper-cloud shield between 4-5 km likely contains liquid water as well as ice clouds, and is therefore likely an elevated area of ascent. A sloping area of dry air ($RH_w$= 30-40%; q = 0.7-2.0 g $kg^{-1}$) descends from west of the upper-level cloud to about 2 km altitude beneath the upper-level clouds. This is likely an area of strong subsidence. Some dry air ($RH_w$ ~70%) is noticed even below this level, reaching almost to the ocean surface immediately west of the surface front. The area of $RH_w$ > 100% just east of the front at 1.5-2.2 km altitude (below the freezing level) likely marks the main, strong frontal updraft, and hence is likely an area of ample liquid water. The low-level moist regions at the western end of the cross-section in Fig. 3a are only associated with a narrow region of relatively shallow clouds

The moist region near the western edge of the upper-level cloud shield is also a region of enhanced baroclinicity between 3.8 and 5.3 km (Fig. 4), and marks the location of the upper-level jet (Fig. 5a). The low-level jet near 1 km in the warm sector appears to have a thin link to the upper-level jet, extending from the upper-level jet to the warm sector along the front. However, because of the coarse spatial resolution of the data, this conclusion is tentative. The diagnosed frontal position in the cross-section is supported by the $\theta_e$ field as well as the wind direction field (Fig. 5b).

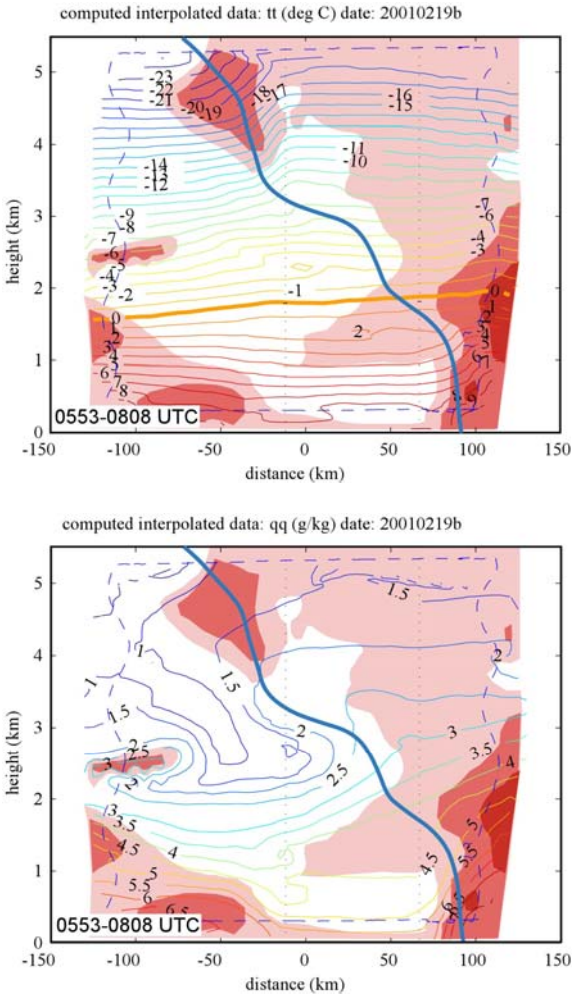


*Fig. 2: W-E cross section analyses from the flight-level data and 2 dropsondes between 0553-0808 UTC Feb. 19, 2001. The flight track is shown by the blue dashed lines, and the dropsonde locations are shown by the vertical dotted lines. The isopleth fields shown are a) temperature (T) and b) mixing ratio (q). The front, determined primarily from the $\theta_e$ field (see Fig. 4) is shown as a heavy blue line, and the three intensities of the color shading represent $RH_w$ ≥ 80%, 90%, and 100%, respectively. In a), the 0°C isopleth is thickened.*

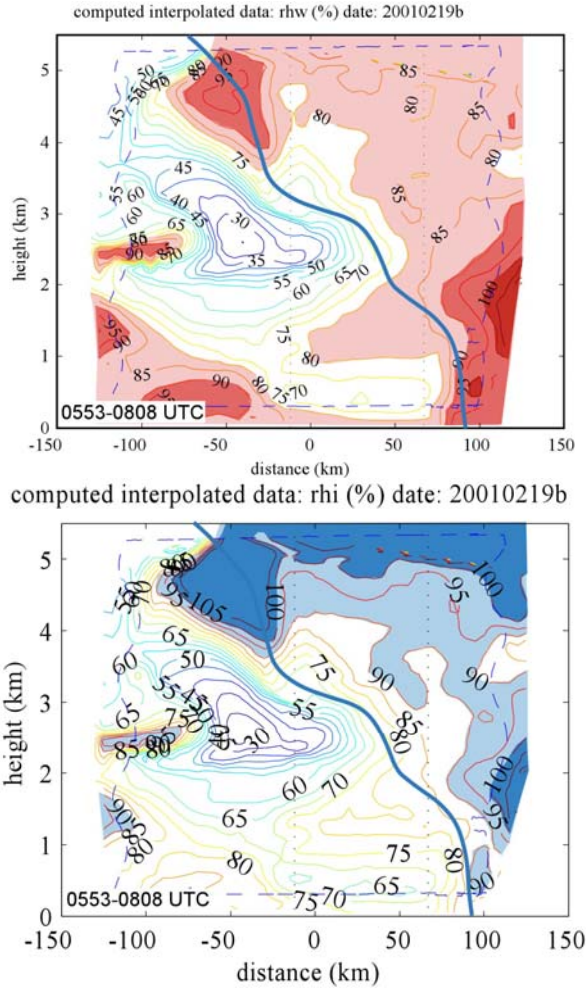


*Fig. 3: Same as Fig. 2 but showing isopleth fields of a) relative humidity wrt water ($RH_w$), and b) relative humidity with respect to ice ($RH_i$). In a, the three intensities of the red shading represent $RH_w \geq 80\%$, 90%, and 100%, respectively, while in b) the two intensities of the blue shading represent $RH_i \geq 90\%$ and 100%, respectively.*

.

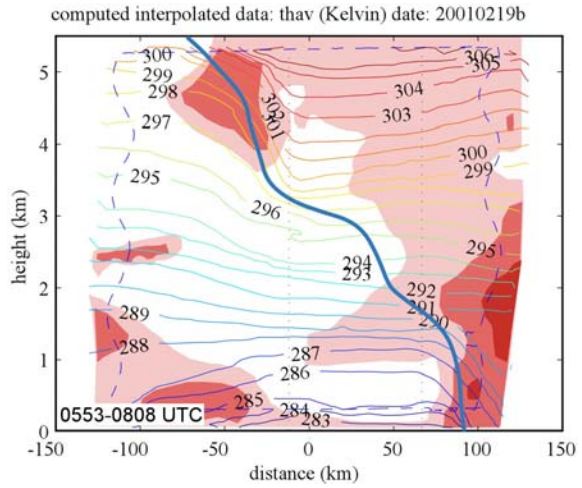


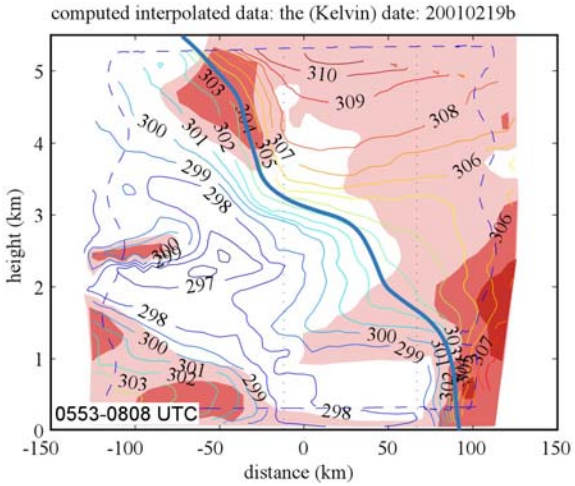


*Fig. 4: Same as Fig. 2 but showing isopleth fields of a) $\theta_v$ and b) $\theta_e$.*

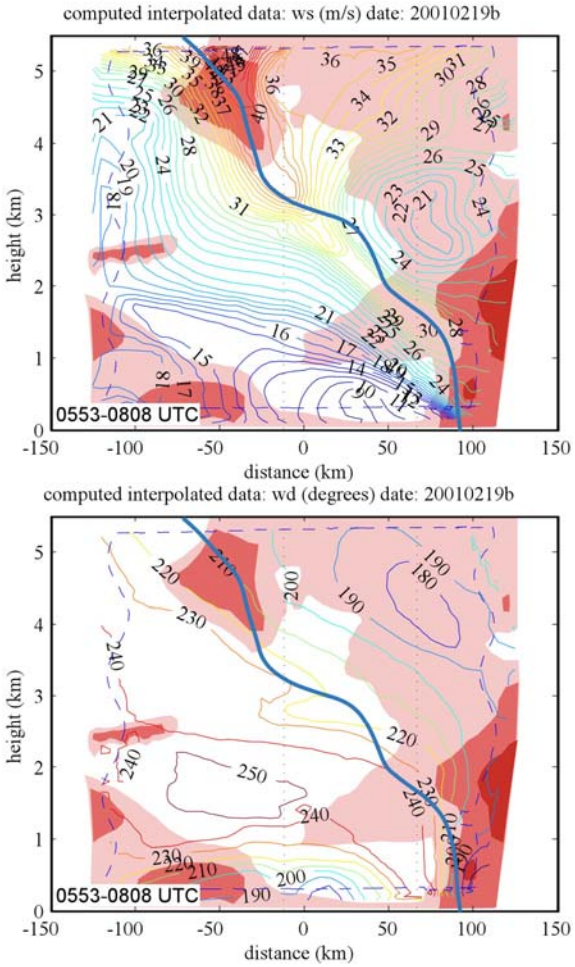


*Fig. 5: Same as Fig. 2 but showing isopleth fields of a) wind speed and b) wind direction.*

### 2.2.2 Radar analyses of the frontal and post-frontal regions

The tail radar reflectivity data show the classical core and gap structure of the NCFR (Fig. 6), with reflectivities in the cores exceeding 50 dBZ. The winds are southerly ahead of the surface front and west-southwesterly behind it. Though the observations were made at slightly earlier, the radar fields were moved to a position at 06 UTC using the phase velocity in order that a direct comparison with the model output could be made.

The vertical cross-sections through the NCFR and the precipitation region behind it (Fig. 7) shows that the strong reflectivities reached an altitude of about 3-3.5 km and that weaker precipitation was present up to nearly 6 km above the main NCFR. The NCFR is 5-7 km wide. The high wind speed field suggests a connection between the strong winds aloft and the LLJ east of the front as noted in the analysis of the in-situ data. However, the radar provides information within 20-30 km of the front and on a smaller scale than obtained from the in-situ data. As is frequently seen in NCFRs the wind direction field indicates the presence of a "head", suggesting that the post-frontal air is behaving at least partially like a density current (e.g., Carbone 1982; Hobbs and Persson 1982). The vertical velocity field shows a maximum updraft velocity of nearly 6 m $s^{-1}$ reached at an altitude of 2.2 km near the height of the observed "head". The reflectivity field also indicates a prefrontal bright band at 1.5 km and a post-frontal bright band at 1.1 km, which

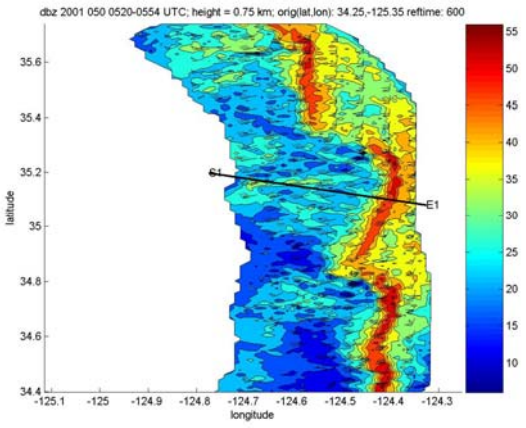


*Fig. 6: Reflectivity (dBZ) and horizontal wind barbs at 0.75 km altitude from P-3 tail radar between 0520-0554 UTC, Feb. 19, 2001. The line S1-E1 shows the position of the cross section in Fig. 7. The position of the NCFR is that at 06 UTC.*

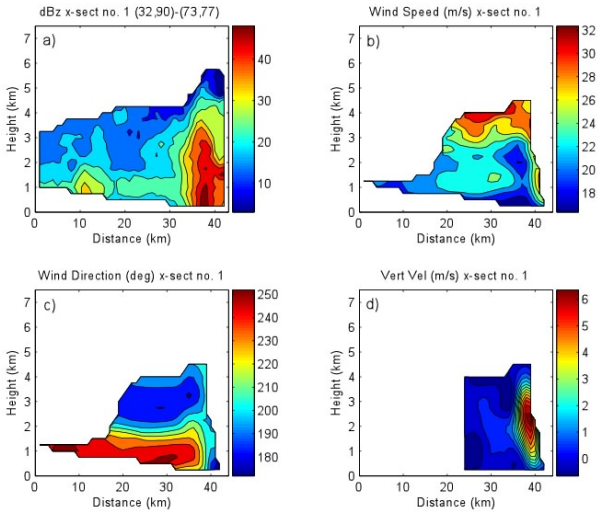


*Fig. 7: Radar-derived fields of a) reflectivity, b) wind speed, c) wind direction, and d) vertical velocity along the cross-section S1-E1 shown in Fig. 6.*

appears to be about 0.5 km below the zero-degree isotherm shown in section 2.2.1.

## 3. MODELING

### 3.1 MODEL DESCRIPTION

The MM5 simulation of this case used 4 nests with resolutions of 45, 15, 5, and 1.7 km, respectively. The finest mesh consisted of 248 X 448 grid points. Fifty-one sigma layers were used, with 22 of them located below 850 mb. This fairly large number of layers maintained an adequate grid-spacing aspect ratio, allowing the use of the 1.7 km horizontal resolution without initiating any obvious numerically generated gravity waves (Persson et al 1991). This fine resolution is marginally adequate to resolve the 5-7 km width of the NCFR. The three outer domains were initialized at 00 UTC Feb. 18 and run for 48 hours. The finest mesh was initiated at 17 UTC Feb. 18 and run for 22 hours. The period 04-09 UTC Feb. 19 is the crucial period for the aircraft validation.

Explicit microphysics was treated with the NASA Goddard microphysics scheme (Tao and Simpson 1993) for each domain. The Grell cumulus parameterization (Grell et al 1995) was applied in the 45-km and 15-km domains, while no cumulus schemes were used in the 5-km and 1.7-km domains. The Eta model PBL scheme was also used.

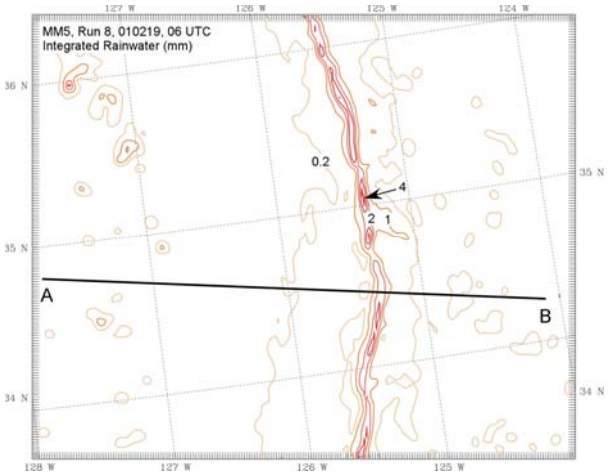


*Fig. 8: Integrated rainwater (mm) at 06 UTC Feb. 19, 2001, for the MM5 simulation. The line A-B shows the position of the cross-section shown in later figures.*

### 3.2 MODEL VALIDATION

The NCFR is clearly represented in the simulation, though the frontal position is about 1 degree too far west (phase velocity is too slow) in this 30 hour forecast (Fig. 8). The integrated rain water field shows the presence of gaps and cores in the simulation. The simulated cores have approximately the correct along-frontal scale when compared to the observed cores.

Vertical cross-sections through the simulated NCFR (along line A-B) are done to validate the simulated vertical structure (Figs. 9-12). The position of the frontal surface in the cross-section is found by examining the fields of $\theta_e$ and winds (Fig. 9) in a manner similar to that used for the observations in section 2.2.1. The simulated front has approximately the same slope as the observed one, as they both reach 5 km altitude (~480 mb) about 150 km to the west of the surface front. Low relative humidity air descends in a sloping manner behind the front, reaching the top of the boundary layer, again in agreement with the observations. However, the local enhancement of the relative humidity observed near the frontal surface at 4-5 km altitude is not present in the simulation. Though there is enhanced baroclinicity in this region, there is no evidence of convergence or enhanced lifting in this region (Fig. 10). Local regions of convergence and enhanced lifting do occur at other locations along and above the sloping frontal surface within the upper level clouds of this system.

The vertical structure of the wind field is also reasonably well simulated by the model (Fig. 11). The simulated winds at 1-1.5 km altitude (900-850 mb) just ahead of the front are 28-32 m $s^{-1}$, which is similar to those observed. However, other radar and in-situ analyses exist that show that the intensity of the LLJ and its horizontal extent into the warm sector is not adequately represented in this cross-section from this

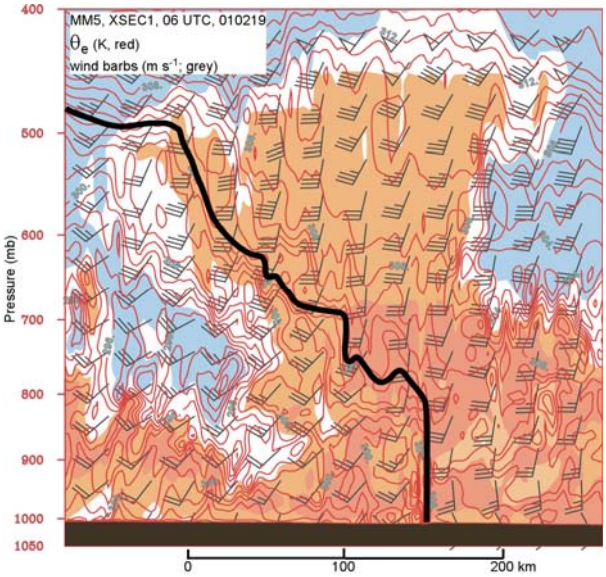


*Fig. 9: Vertical cross-section along line A-B in Fig. 8. The cross-section shows equivalent potential temperature ($\theta_e$, K, red contours) and horizontal wind barbs. The background shading shows the relative humidity with respect to water, with RH > 95% in red, 76%<RH<95% in brown, and RH<38% in blue. The heavy black line is the position of the frontal surface estimated from the $\theta_e$ and wind field (see text).*

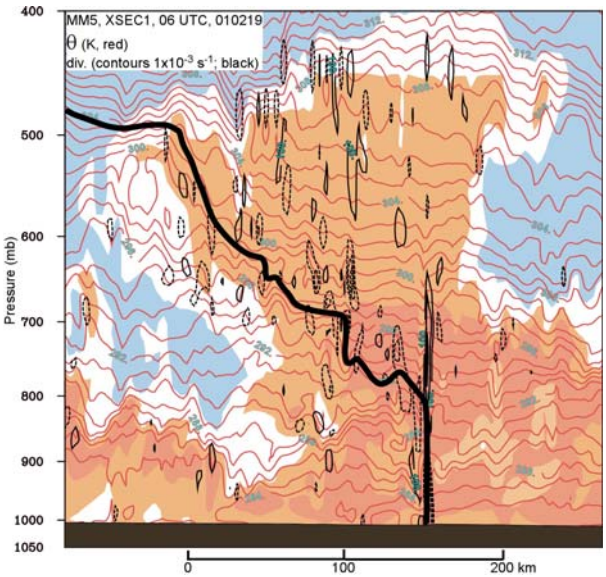


*Fig. 10: As for Fig. 9, but showing potential temperature ($\theta$, K, red isopleths) and horizontal divergence (isopleths of 1 x $10^{-3}$ $s^{-1}$; black isopleths).*

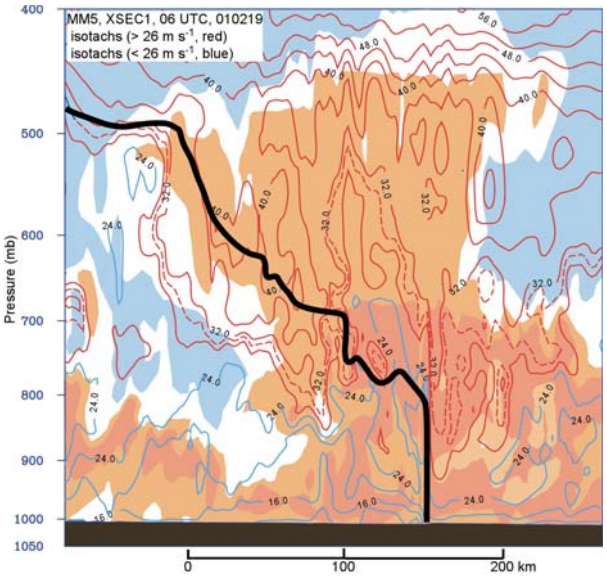


*Fig. 11: As for Fig. 9, but showing wind speed (red isopleths are for > 26 m s$^{-1}$ and blue isopleths are for < 26 m s$^{-1}$).*

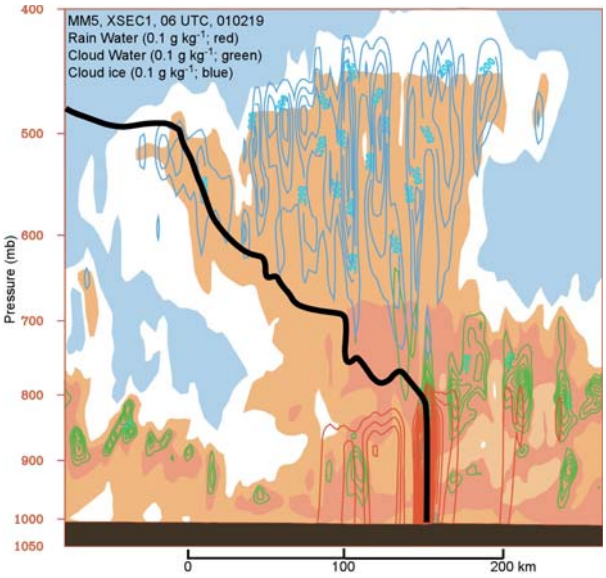


*Fig. 12: As for Fig. 9, but showing the mixing ratios of the microphysical quantities rainwater (red), cloud water (green), and cloud ice (blue).*

simulation. The winds aloft near 5 km range from 32-40 m s$^{-1}$, slightly weaker than those observed. While the strongest winds in the simulation at 5 km altitude do occur near the frontal surface, the simulated winds are only 40 m s$^{-1}$ while the observed winds reach 48 m s$^{-1}$. A tongue of stronger winds does descend along the sloping cold front in the simulation in agreement with the observations. However, this high velocity air descends to the boundary layer behind the frontal surface, being separated from the LLJ and the frontal head by a plume of lower momentum air just to the rear of the main updraft. The high momentum tongue from aloft, the plume of lower momentum air are present within 30 km of the surface front, so this simulated structure seems to be contradicted by the analyses of both the in-situ and the Doppler radar data.

The microphysical fields (Fig. 12) show the vertical extent of the heavy precipitation associated with the NCFR extending to 2-3 km, in reasonable agreement with the observations. Updraft cells aloft produce numerous ice clouds above the frontal surface. Some of the liquid water clouds in the warm sector are also able to produce surface precipitation.

## 4. CONCLUSIONS

A fine-scale simulation of a convective cold front observed over the Pacific Ocean is validated with in-situ and radar observations obtained from the NOAA P-3 aircraft. In general, the simulation appears to be quite good, though differences in some details exist. Whether these differences are due to local along front variations needs to be explored. Also, further analysis is needed to resolve whether these differences are important when comparing this simulation to the TRMM satellite observations.

**Acknowledgements**

This work was supported by a grant from National Aeronautics and Space Administration's (NASA's) Goddard Laboratory, by NASA Grant NAG5-10790, and by NOAA's Oceanic and Atmospheric Research.

## 5. REFERENCES

Carbone, R. E., 1982: A severe winter squall line. Stormwide hydrodynamic structure. *J. Atmos. Sci*., **39**, 258-279.

Grell, G. A., J. Dudhia, and D. R. Stauffer, 1995: A description of the fifth-generation Penn State/NCAR Mesoscale Model (MM5). NCAR Tech. Note TN-398+STR, 122pp.

Han, M., S. A. Braun, P. O. G. Persson, and J.-W. Bao, 2005: A modeling study of the along–front precipitation variability of a Pacific narrow cold frontal rainband. *Preprints on CD-ROM, 32nd Conference on Radar Meteorology,* Amer. Meteor. Soc., 24-29 October, 2005, Albuquerque, NM, paper JP4J.2.

Hobbs, P. V., and P. O. G. Persson, 1982: The mesoscale and microscale structure and

orgnaization of clouds and precipitation in midlatitude cyclones. Part V: The substructure of narrow cold-frontal rainbands. *J. Atmos. Sci*., **39**, 280-295.

Jorgensen, D. P., Z. Pu, P. O. G. Persson, and W.-K. Tao, 2003: Variations associated with cores and gaps of a Pacific narrow cold frontal rainband. *Mon. Wea. Rev*., **131**, 2705-2729.

Persson, P. O. G., B. Walter, and J. Hare, 2004: Maritime differences between wind direction and stress: Relationships to atmospheric fronts and implications. CD -ROM of *Preprints, 16th Symposium on Boundary Layers and Turbulence*, 9-13 Aug, Portland, ME.

Persson, P. O. G., and T. T. Warner, 1991: Model generation of spurious gravity waves due to the inconsistency of the vertical and horizontal resolution, *Mon. Wea. Rev.*, **119**, 917-935.

Rotunno, R., J. B. Klemp, and M. L. Weisman, 1988: A theory for strong, long-lived squall lines. *J. Atmos. Sci.*, **45**, 463-485.

Tao, W.-K. and J. Simpson, 1993: The Goddard Cumulus Ensemble Model. Part I: Model description. *Terr. Atmos. Oceanic Sci.*, **4**, 35-72.